International Journal of Latest Engineering and Management Research (IJLEMR)
ISSN: 2455-4847
www.ijlemr.com || Volume 07 - Issue 03 || March 2022 || PP. 01-11

Heat transfer and fluid flow Investigationfor annulus with inner twisted elliptic and outer plane tubes

Ali Abduladheem Hilal
M. Sc. Studeny, mechanical engineering, Al-Nahrain University, Baghdad, Iraq
Al-Furat Al-Awsat Technical University, Iraq

Ahmed F. Khudheyer
Al-Nahrain University, Baghdad, Iraq
drahmed955@eng.nahrainuniv.edu.iq

Abstract: Heat transfer performance of a new concentric tube made by plain and twisted elliptical tubes is quantitatively explored. For consistency's purposes, a ring made from two plain elliptical pipes is also examined. Interior twisting oval tubes with different orientations and twisting fractions were explored. The asymmetrical flow pattern in the annular greatly enhances heat transmission. In the examined range of design variables, the Nusselt number typically rises as the interior curved tube flattens and the twisting get more pronounced. In comparison to an internal smooth pipe, the interior helical tube's greatest Nusselt number Nu rises by 116%, but the skin friction coefficient f only rises by 46%, and the thermophysical properties index (JF) may rise to a maximum of 1.9. Using the Nusselt number and friction factor, it is possible to derive correlations between the two for turbulent flow, with error margins of 5 per cent and 4 per cent, correspondingly.

Keywords: ellipsoid twisting tubes, pipe concentric, Exchanger with inner and outer tubes, thermal performance, elliptic tubes.

1. Introduction

DOUBLE PIPE HEAT EXCHANGERs are extensively used in a variety of energy fields because they are simple, easy to clean, or have a diverse spectrum of applications [1]. Optimizing that DOUBLE PIPE HEAT EXCHANGER's efficiency is critical for saving energy. Thermal performance augmentation may be accomplished in two ways: actively or passively. External power is required for active methods like ultrasonic irradiation [2] or magnetic fields [3–5]. To generate high secondary flow, passive methods such pipe inserts [6,7], vortex producers [9–11] and specially formed pipes [12–14] have been shown to be beneficial for heat generation [15–19]. These include features and capabilities, vortex producers, as well as particularly unique tubes. It is these low-cost passive methods, along with greater stability and dependability, that are the most often used in DOUBLE PIPE HEAT EXCHANGER.Pipe inserts may actively enhance the heat transmission within the tubes. For self-rotating helical coil, Zhang et al. [6] discovered that perhaps the Nu and f rise with increasing perforations ratios. Whenever the penetration diameter was 5 mm, highest improvement factor of 1.07 was reached by Mashoofi et al. [7], who development takes that the greater heat transfer results are achieved by longitudinally punched tape that plain tape inserts. Researchers Esmaeilzadeh et al. [20] found that adding helically coiled plugs to a circular pipe significantly improved the round tube's convection heat transmission. Man et al. [21] empirically investigate the thermal of such a twisted tapes as well as observed that both Nu and f enhanced considerably. By using the perforations features and capabilities with the best shape, Sheikholeslami and Ganji [8] found that at Reynold's number (Re), overall thermal efficiency factor (JF) may reach 1.59. Numerous turbulators designs exist apart from tube plugs to improve heat transmission. In their computational and experimental studies, Bhadouriya et al. [24] examined that thermal efficiency of an annulus tubes with an internal twisting rectangular section. Increasing Re or Pr raises the Nu whereas increasing the twisting ratio lowers it. Three wavy tubing with varying wave frequency and amplitude were analyzed numerically by Bashtani and Esfahani [25]. They found that about an equal length portion, the maximum Nu was 1.75 times bigger. Computational studies by Zambaux et al. [26] examined the heat transmission properties of an annulus tube with periodic wall permanent deformation upon both opaque and transparent tube walls. When the longitudinally sequence of the tubes was equivalent approximately 1/8, the quantity of JF may reach up to 1.43. An outwardly helix wavy tube has been used as a inner tube in a numerical study by Wang et al. [27]. They discovered supplementary or whirling flows just on tubes with shell's edges, with a shell radius of 19 mm providing the best geometrical characteristic. An analysis by Gorman et al. [28] showed that the spirally ribbed double pipe heat exchanger had a rate of heat transfer 4 times greater and a pressure loss two times lower than that of a basic, softly double pipe heat exchanger. According to ref. [29], with wavy pipe outperforms a double pipe heat exchangerwith such a plain tube in terms of total effectiveness. Many studies have looked just at

geometric features of something like the double pipe heat exchangers, even though the exterior tubes are almost always circular. Double pipe heat exchangerexterior plain tubes or double pipe heat exchanger inner twisting elliptical tubes have not been addressed in any published work.

This article proposes a new double pipe heat exchangercircular tube with outside straight and interior twisted elliptical tubes. The effects of inner tube's aspects with twisting percentages on flow parameters and effective thermal conductivity in the concentric tubes were investigated numerically. An interior twisted elliptical tube significantly enhance the thermal effectiveness of the concentric tube. The findings are important for the development of double pipe heat exchangers with superior heat attention to the details.

2. Problem description

Fig. 1 depicts a schematic representation of the concentric tubes under investigation. L approximately 1500 mm long. The external plain elliptical tube's longitudinal dimension (a_0) and transverse axis (b_0) were 41 mm as well as 30.75 millimeters, correspondingly. The throughout some (ai) of the interior oval pipe is fixed at 24 millimeters, whereas the final three planes (bi) measured were 9.6 millimeters, 12 millimeters, and 14.4 millimeters. In this study, three twist ratios (P) were taken into account. For the interior elliptical tube, corresponding twist-to-aspect-ratio equations were s = P/ai and e = bi/ai, accordingly. X = x/P seems to be the dimensionless length. The twisting ratios used in this research were s = 10, 15, and 20, as well as the aspect ratios were e = 0, 4, and 6, respectively.

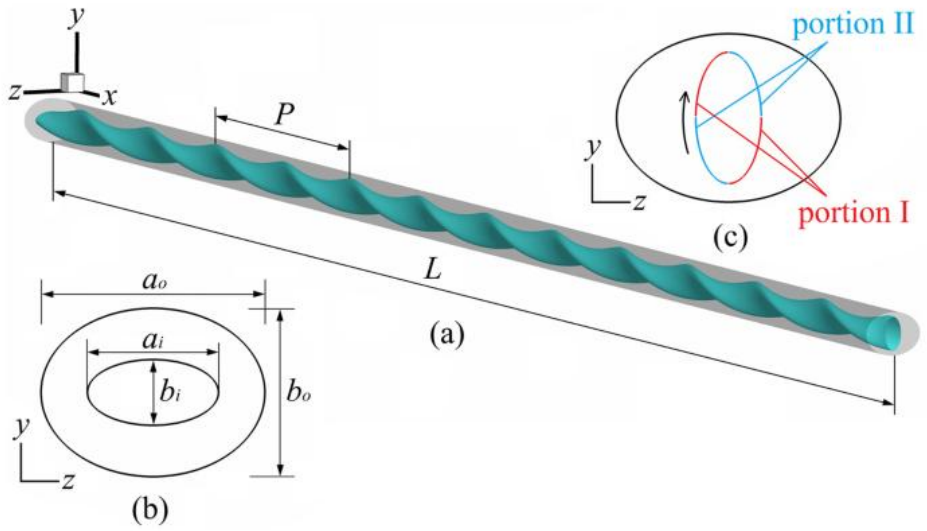

Fig. 1. Schematic diagram, (a) concentric tubes, (b) cross sectional area (c) portions I besides II for elliptical internaltube.

3. Mathematical model

It is assumed that the airflow inside the annular is impermeable to pressure changes but has a Prandtl number of 0.7 in this research. Under steady - state condition, the fluid flow is three-dimensional. All of these things are ignored when computing the angular momentum of an object. Re may range anywhere from 1000 to 15,000, depending on whether the flow is laminar or turbulent. The following seem to be the formulas for continuity, momentum, and energy:

$$\frac{\partial}{\partial x_{\mathrm{i}}}(\rho u_{\mathrm{i}}) = 0 \qquad 1$$

$$\frac{\partial}{\partial x_{\mathrm{i}}}\left(\rho u_{\mathrm{i}} u_{\mathrm{j}}\right) = -\frac{\partial p}{\partial x_{\mathrm{j}}} + \frac{\partial}{\partial x_{\mathrm{i}}}\left((\mu + \mu_{\mathrm{t}})\frac{\partial u_{\mathrm{j}}}{\partial x_{\mathrm{i}}}\right) \qquad 2$$

$$\frac{\partial}{\partial x_{\mathrm{i}}}\left(\rho C_{\mathrm{p}} u_{\mathrm{i}} T\right) = \frac{\partial}{\partial x_{\mathrm{i}}}\left((\lambda + \lambda_{\mathrm{t}})\frac{\partial T}{\partial x_{\mathrm{i}}}\right) \qquad 3$$

Re-normalization Group (RNG) k— "The relatively close treatment method with improved wall treatment can be used for turbulent flow modeling. for the sake of argument, let us assume "a list of them is provided as follows:

$$\frac{\partial}{\partial x_i}(\rho k u_i) = \frac{\partial}{\partial x_i}\left((\mu + \mu_t)\frac{\partial k}{\partial x_i}\right) + G_k - \rho\varepsilon \qquad 4$$

$$\frac{\partial}{\partial x_i}(\rho\varepsilon u_i) = \frac{\partial}{\partial x_i}\left((\mu+\mu_t)\frac{\partial \varepsilon}{\partial x_i}\right) + C_{1\varepsilon}\frac{\varepsilon}{k}G_k - C_{2\varepsilon}\rho\frac{\varepsilon^2}{k} \quad (5)$$

G_k: Average velocity variations induce turbulent kinetic energy generation.

Hydraulic diameter,

$$D_h = \frac{4A}{L_P} \quad (6)$$

$$A = \pi(a_o b_o - a_i b_i) \quad (7)$$

$$L_p = \pi\left(\frac{3}{2}(a_o + b_o) + \frac{3}{2}(a_i + b_i) - (a_o b_o)^{0.5} - (a_i b_i)^{0.5}\right) \quad (8)$$

$$Re = \frac{\rho u_{in} D_h}{\mu} \quad (9)$$

$$f = 2\frac{D_h}{\rho u_{in}^2}\frac{\Delta p}{L} \quad (10)$$

$$h_{local} = \frac{q_{local}}{T_w - T_s(x)} \quad (11)$$

Bulk mean temperature is,

$$T_b(x) = \frac{\iint_{A(x)} u(x,y,z)T(x,y,z)dydz}{\iint_{A(x)} u(x,y,z)dydz} \quad (12)$$

Nusselt number on the inner surface of the tube can be calculated locally as,

$$Nu_{local} = \frac{h_{local} D_h}{\lambda} \quad (13)$$

The average Nusselt number on the interior surface of the tube is,

$$Nu = \frac{1}{S}\iint_S Nu_{local}\, dS \quad (14)$$

S is the inner surface area of tube.

Boundary conditions

The following seem to be the concentric tube boundary conditions:

Inlet :u_{in} = 0.02 m/s, T_{in} = 300 Km turbulent intensity $I=0.16Re^{0.125}$.

No slip conditions, inner surface temperature of the internal tube is 363K while the external surface for the outer tube of the annulus can be considered as adiabatic.

Outlet section: $\frac{\partial u}{\partial x} = \frac{\partial v}{\partial x} = \frac{\partial w}{\partial x} = \frac{\partial T}{\partial x} = \frac{\partial k}{\partial x} = \frac{\partial \varepsilon}{\partial x} = 0$.

Geometry locations	Boundary conditions
Inlet	Velocity inlet, $T = 298.15$ K, $U_x = U_{x,\ inlet}$
Outlet	Pressure outlet, $\frac{\partial U}{\partial x} = \frac{\partial T}{\partial x} = 0$, relative pressure at the outlet is zero
Inner tube wall	Non-slip and uniform constant temperature wall, $T_{wall} = 313.15$ K, $U_x = U_y = U_z = 0$
Outer tube wall	Non-slip and adiabatic wall

4. Numerical analysis:

ANSYS Fluent R2 2020 can be used to model the issue in the annulus tubes using the finite volume technique and the semi-implicit technique with pressure related formulas (SIMPLE). The gradients as well as pressure were calculated using the cell-based technique and an approximation of secondorder, correspondingly. When solving the equations of momentum and heat, use upwind method. Energy equation as well as the other equations have convergence criterion of 10 e-8 as well as 10 e-6 correspondingly.

5. Grid generation and mesh independent

Hexahedral pieces mesh together to form a web that may be used for computational purposes. The annulus tube's micro - grid may be improved using O-grid technique. The turbulent model's scale factor y + seems to be very significant. The first hexagonal wall thickness is influenced by the values of y^+ as well as Re. The y^+-value is set to 1, as well as the relatively close grid's growth factor is 1.2 for all simulations.for Re = 2050, *s = 15*, e = 0.50, and Pr = 0.7, five different grid system quantities were examined to explore grids independently. The results are shown in Figure2. Even as grid size grows, so do Nu and f. Nu and f have relative errors of less than 0.7 percent and 0.3 percent, correspondingly, between both the 4,113,120 to 5,100,440 grids. When selecting a grid system, the matrix size, stability, and calculation convergence time are all taken into account. This grid has s = 15 and e = 0.5, as seen in Figure 3. To ensure the accuracy of the obtained approach,

Bhadouriya et al. [24] used the same model properties and model parameters in their experiment to confirm the numerical findings. For laminar flow with Re = 1000, the error percentage of fRe is 5.5 percent, whereas for turbulent flow with Re = 12,000, the relative error is 11.4 percent, as shown in Table1. As a consequence, when compared to the empirical observations, the numerical values are appropriate.

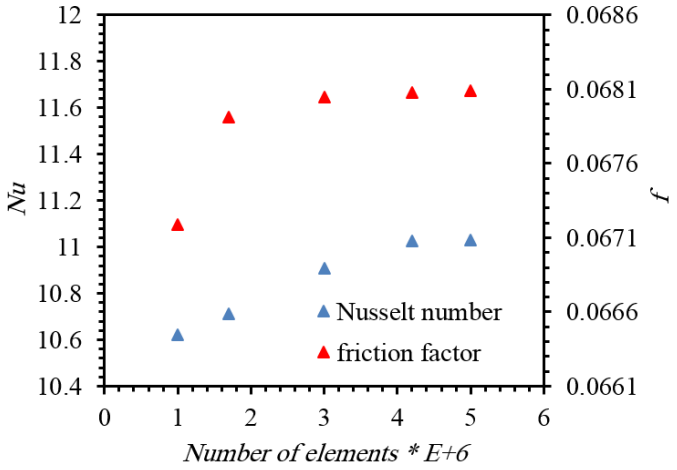

Figure 2. Mesh independence

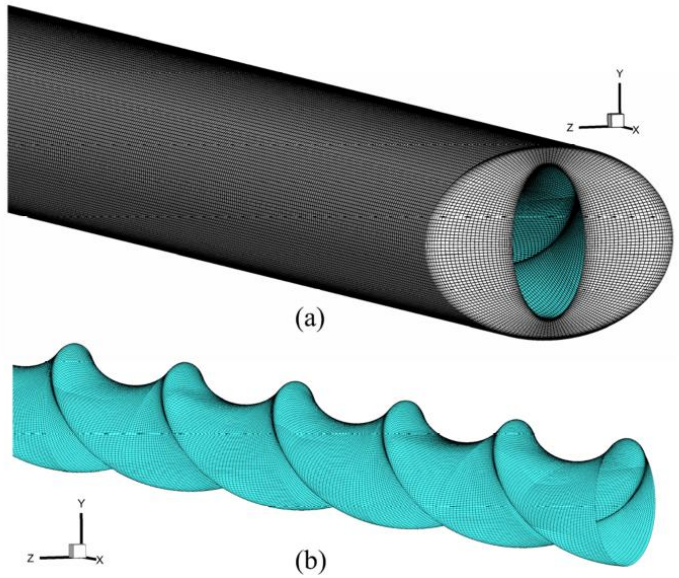

Figure 3. Grid system: (**a**) grid of outer tube and cross section, (**b**) grid of inner tube.

Table 1. Validation of present study.

Calculation Model	Laminar, *Re* = 1000		RNG *k*–ε, *Re* = 11,000	
	fRe	*Nu*	*fRe*	*Nu*
Experiment [24]	22.7	4.41	87.4	43.31
Present	21.45	4.01	97.39	38.67
Relative error	5.5%	9.1%	11.4%	10.7%

6. Results and discussion

6.1 fluid flow features

For different values of e and s, typical auxiliary flow mostly in annular is shown in Figure 4 with Re = 3000. Figure 1c represents the central elliptical tube's part I and II pipe walls labeled as segment I and II, respectively.

The outcome of the simulation with an internal smooth pipe can be seen in Figure4a as a point of comparison. That secondary flow in Figure4a was minimal due to the straightness of the external as well as

inner pipes. Figure4a's velocity caption has already been magnified by a factor of 300 compared to the previous figures. Secondary flow with a high tangential velocity becomes evident due to the inner twisting elliptical tube. The annular center rotates symmetrically with respect to the secondary flow upon that cross - sectional area. According to the interior tube's twisted, fluid with a velocity tangentially of high flows over section II with surface as well as splits first from tube somewhere at quick endpoints. Figure4b–d shows that when e decreases from 0.6 to 0.4, the secondary flow produced by the twisted internal diameter rises. The flow separation weakens as s increases because the torsional distortion of the internal twisting tube decreases, as illustrated in Fig.4.

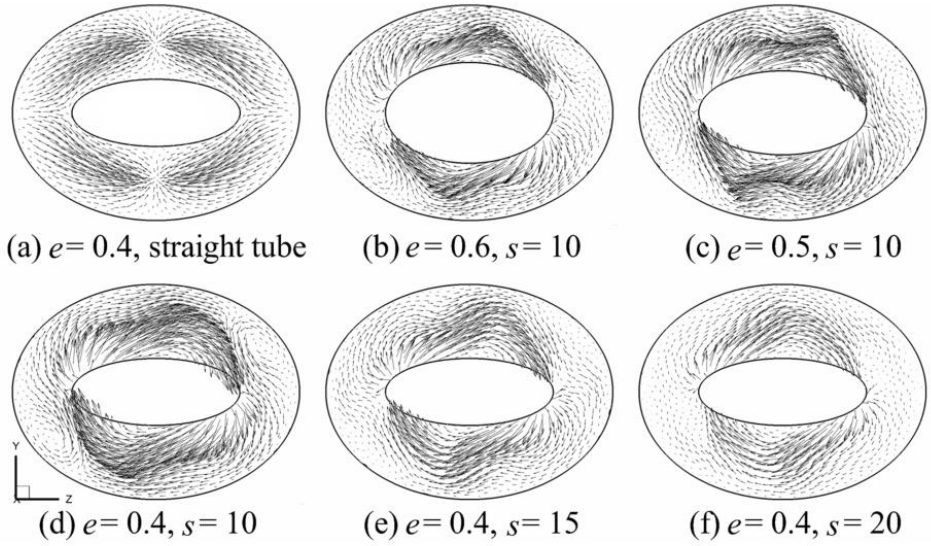

Figure 4. Comparison of secondary flow for different e and s at x = 720 mm with Re = 3000.

Figure 5 illustrates the flow pattern upon that third warped pitched period started cross - section for s = 10, Re = 3010, and e = 0.4. Figure 5 illustrates the ancillary flow. Internal elliptical tubes twisted were twisted clockwise from 0 to 360 degrees with such a 45-degree increment to choose the cross - section. With a twisting inner elongated tube, there are distinct distributes of secondary flow because the annular created by outside plain versus inner twisting elliptical tubes has always been altering.

The fluid travels across the direction extremities before reversing course in section II owing to the oblong tube's turning. As seen in Figure 5a–e, the velocity profile rises in section II as even the twisted angle varies from zero to 90 degree angle, and afterwards decreases as that of the turning angle climbs continuously from 90 to 180 degrees. The reason for this is because when the twisted angle (0 to 90) degrees, the distance between both inner and external tubes becomes smaller until they are perpendicular to each other. the annular interplanetarybe situatedleast, the velocity tangentially achieves its maximum rate, illustrated in Fig.5c. When s = 10, Re = 3010 and e = 0.4are used, a tangential velocity decreases as even the space increases. The inner elliptical tube twisting were twisted clockwise from 0 to 360 degrees with a 45-degree interval to choose the cross sections. There are distinct secondary flow distributions owing to the shifting annulus created between the outer regular and inner bent elliptical tubes, generated by inner twisting elliptical tube.

Because of the oval tube's twist, fluid flows over the long axis extremities and changes shape in section II. As seen in Figure 5a–e, the angular momentum rises in section II as the twisted angle varies from zero to 90 degrees, but then decreases as the twisting angle climbs continuously from 90 to 180 degrees. With increasing twisting angles from 0 to 90 degrees, the distance between inner and outer tubes becomes smaller. The distance is lowest when both oval tubes' transverse axis is orthogonal to one another.

Figure 5c shows that the velocity profile is greatest when the annular space is smallest. Whenever the twisting angle goes from 90 to 180 degrees, the tangential velocity falls as the volume increases. When the twisting angle is between 180 and 360 degrees, the secondary flow variations in Figure5e–i seem quite comparable to that in Figure5a–e, where the twisted ratio distributions were between 0 and 180 degrees. 90-degree to 180-degree angle shifts occur. When the turning angle is between 180° and 360°, the secondary flow patterns in Figure 5e–i seem quite similar to others in Figures 0–180°.

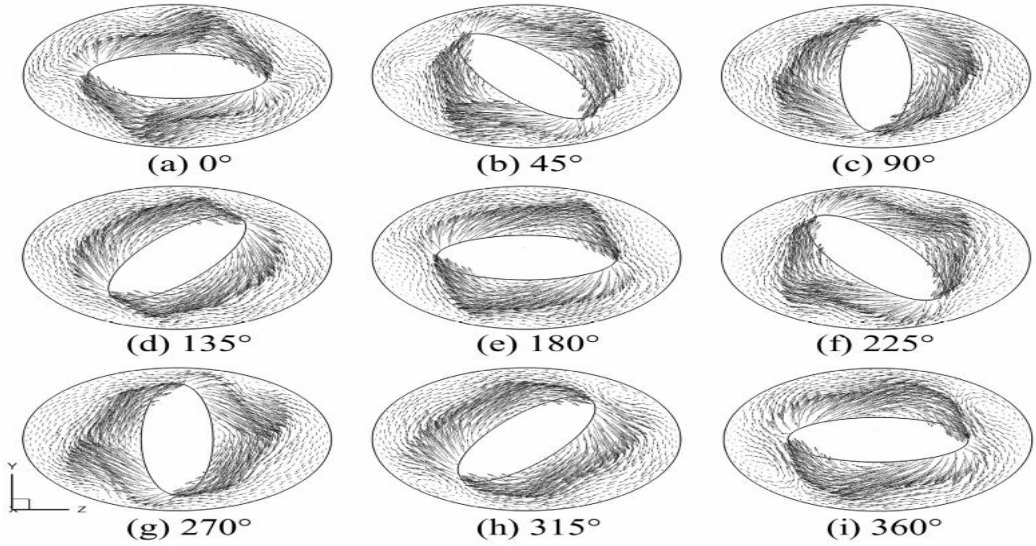

Figure 5. Secondary flow of the third twisted pitch period for $e = 0.4$, $s = 10$ at $Re = 3000$.

6.2 heat transfer characteristics

At an identical x = 720 mm location, Figure6 shows the cross-sectional thermal behavior in a similar fashion. For comparison's convenience, the temperature field of the annular is also depicted with an internal straight pipe.

On the inside also displayed for comparison has been the annulus' temperatures field with an internal smooth pipe. The fluid flows rotationally via the inner twisted oval tube and produces a secondary flow that improves fluid interaction in the annular. The heat in the model's annulus seems to be higher when the inner layer is distorted than when it is straight. In addition, the inner twisted tube's temperature contours are rotationally symmetric around the tube's core. In Figure 6b–d, for example, the cross-sectional temperatures will be the same s = 10, but the aspect e will vary from 0.4 to 0.6.When e is reduced from 0.6 to 0.4, the thermal zone with such a low value becomes colder. When e lowers, the temperature differential in section II rises from around where the interior tube's direction ends. The reason for this is that when e is low, the temperature profile layer on that inner pipe wall is much more easily damaged by high velocities and secondary flow. Aspect ratio e = 0.4 has been used in Figure 6d–f to show the impact upon that temperature profile caused by the parameter s. As s rises, the twisting tube becomes more straight, which reduces fluid mixing because secondary flow is reduced. Improvements in s. assess lead to a rise in the temperature region with a minimal value, while the fluid mixing reduces owing to a reduction in secondary flow. The low-temperature zone becomes hotter as you go closer to it. The temperature distribution throughout the inner tube surface differs significantly. Each section's temperature fields are symmetrical around the tube's central axis. The inner oval tube has a temperature gradient that is greater near part II than it is near portion I, with the lowest gradient occurring at the short axis ends of the inner oval tube. As a result, the fluid with a low temperature changes direction and has a high tangential velocity along section II. When fluid flows from the long axis ends to the short axis ends, the temperature progressively rises along part II, and then the hot fluid flows across portion I from the short axis ends of the inner tube. Because of this, the temperature surrounding section I of the inner tube is much greater than the temperature around section II as shown in Fig. 7.

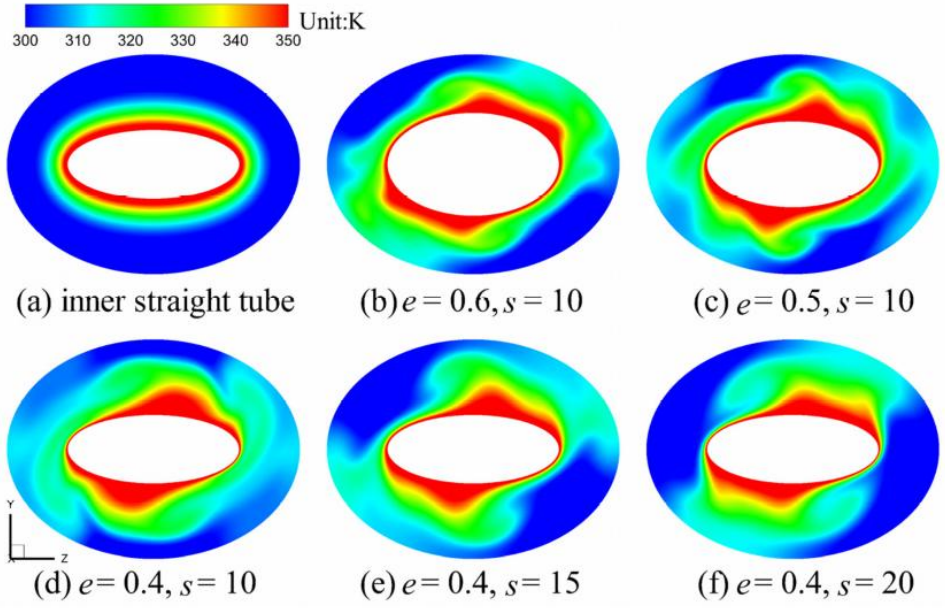

Figure 6. Temperature fields for different e and s at x = 720 mm with Re = 3000.

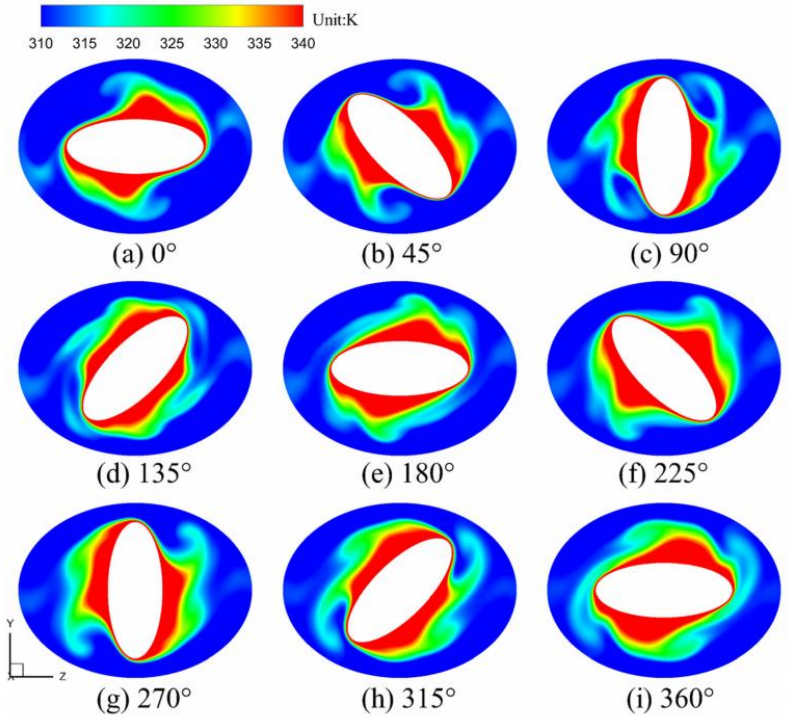

Figure 7. Temperature fields for cross sections of the third twisted pitch for e = 0.4, s = 10 at Re = 3000.

Figure8a shows the Nu distributions for various s with the same inner twisted tube e = 0.4. Nu for the annular tube with an inner straight tube comparison is also provided. When the flow is laminar, the inner straight tube's Nu rises gradually with increasing Re. When the flow is turbulent, the Nu increases rapidly. Then, as the flow becomes more turbulent, Nu rises gradually once again. Nu rises dramatically with increasing Re in both laminar and turbulent flow regimes. The greatest rise in Nu comes when the flow undergoes turbulence, which happens at the transition Re. While both inner tubes have a Nu of 1, they have a considerably lower Nu of 0. In laminar flow, the difference in Nu between annuli with straight and twisted inner tubes grows with increasing Re, while the difference in the turbulent regime is not that significant. This means that under the laminar regime, the inner twisted tube may significantly enhance the annulus' heat transmission. In the case of smaller s inner twisted tubes, nu rises as s lowers because a larger secondary flow may be produced, which

enhances heat transmission. Turbulent flows have larger variations in Nu between them than laminar flows, with a 26 percent difference between them. The greatest Nu of the twisted inner tube rises by 116% and 27% in laminar and turbulent flows, respectively, compared to the case with an inner straight tube.

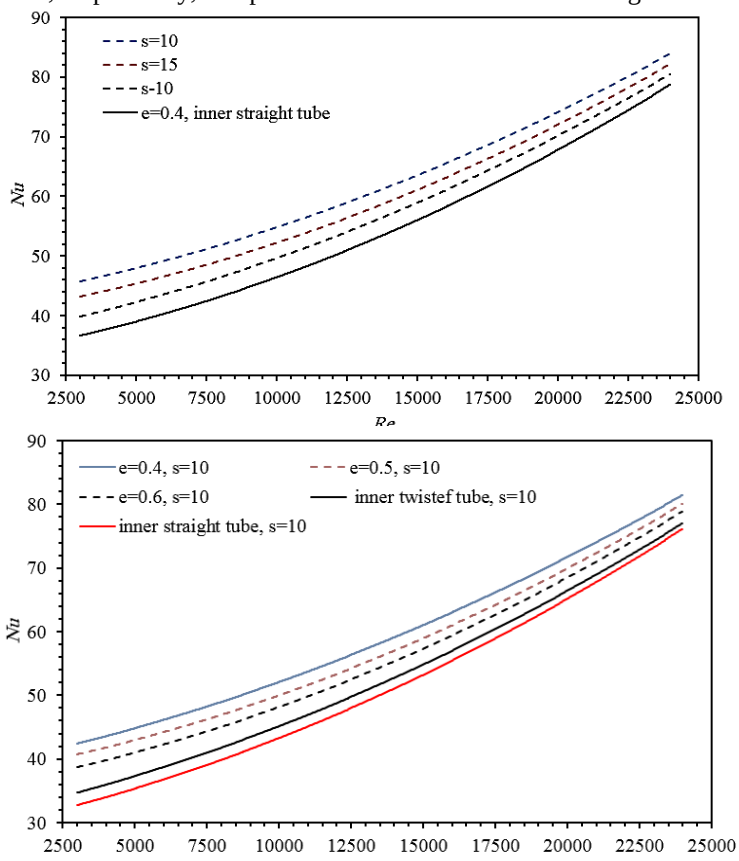

Fig.8 comparison of Nu for different s and e

As you can see in Figure 8b, Nu is compared for various aspect ratios with the same s = 10. Figure 8b shows Nu comparisons for several aspect ratios, all with the same s = 10.

As Re rises, Nu increases for all annular tubes. The inner straight tube has a minor difference in Nu when e is changed, while the inner twisted tube has a large difference in Nu when e is changed. For this reason, as shown in Figure 4, the secondary flow intensity difference produced by an inner twisted oval tube with varying e is vastly different.

The previous research [19] found that the secondary flow intensity is Nu. Since secondary flow in the annulus is considerably greater in the twisted tube, its value is much higher than in the straight tube's inner diameter. Because the torsional deformation of the twisted oval tube's inner wall reduces with increasing twist ratio and secondary flow in the annulus, nu decreases as e increases from 0.4 to 0.6. At s = 10 and Re = 2000, the difference in Nu between various inner twisted tubes is 35%, whereas the difference in Nu between different inner straight tubes is less than 6%. There is an increase in Nu of 116%, 97%, and 82% compared to the comparable straight tubes in the laminar regime, as well as an increase in Nu of a whopping 27%, 21%, and 15% compared to the straight tube.

Figure9a shows the f distributions for various s and the f distribution for the inner straight tube. Different values of s have different f values, and the value for the inner straight tube is clearly larger. When Re exceeds 3000, laminar flow transforms to turbulent flow, and the f for turbulent flow is greater than the f for laminar flow. As s drops, so does the inner twisted tube's f. With *s = 10* and *s = 15 at Re = 3000*, there is an 11.3 percent difference in the f, but with s = 15 and s = 20, there is only a 6.4 percent difference. Most of the 18 percent difference in f is between the two divisors for different values of e (0.4) and Re (3,000). Figure 9b compares the value of f for various aspect ratios using the same *s = 10* as in Figure 8. In both laminar and turbulent regimes, the f of all models reduces as Re increases. f for the twisted inner tube reduces as e increases, while f for the straight inner tube differs very little as e changes. The reason for this is because the secondary flow intensity produced by twisted tubes of different e has a significant variation.

Even though interior convoluted pipes having s = 10 vary by roughly 13 percent, the variation would be less around 4 percent between interior straight tubes. For s = 10, e = 0.4, and Re = 4000, the biggest variation in f is 46% here between interior twisting versus straighter tubing. Define various plain tubing only vary by around 4%. By contrast, the greatest variation in f is seen at s = 10 and e = 0,4 and Re = 3000, where the innermost twisting and regular pipes diverge by 46%.

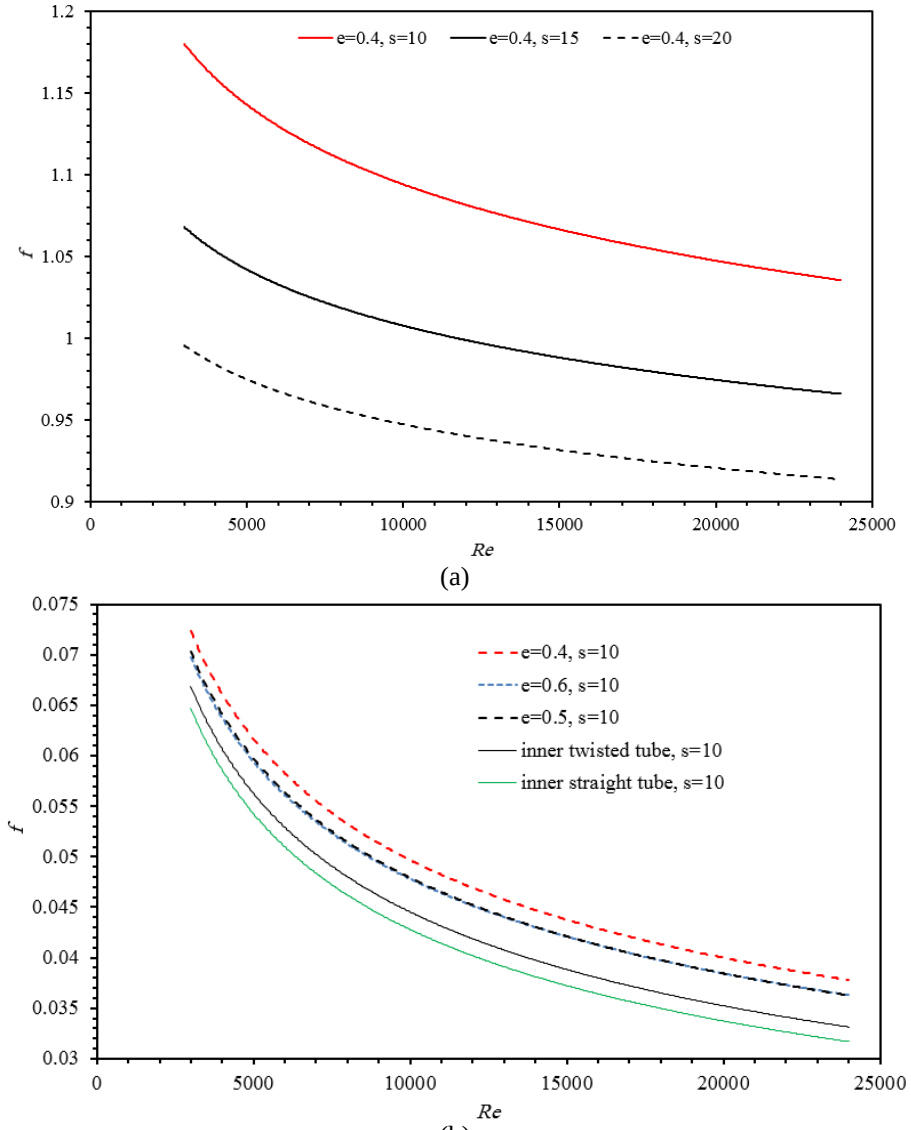

Figure 9. Comparison of *f* for different *s* and *e*: (a) different *s*; (b) different *e*.

Correlations

The best fitted correlations for heat transfer and friction factor in the region of turbulent flow that had been founded here in this article can be shown as,

$$Nu = 0.79458Re^{0.38104}\, e^{-0.59774}\, s^{-0.31025}$$
$$f = 32.02667Re^{-0.81161}\, e^{-0.25102}\, s^{-0.22145}$$

Conclusions

Analysis of thermal conductivity in a new annulus was carried out numerically. The annulus is made up of two twisted oval tubes, one on either side of the ring. The following is a list of the most important findings.

1. The interior twisting elliptical tube clearly improves fluid mixed in the annular.
2. When the aspect ratio and the twist ratio are reduced, nu and f become larger. There are 37.4 percent and 11.7 percent, respectively, increases in Nu and f when comparing various aspect ratios, as well as 24.9 percent and 19 percent, respectively, when comparing different twist ratios.

3. Three times as many nuclei and four times as many fluorophores are produced by the inner twisting oval tube as by the inner straight tube.

References

[1]. Omidi, M.; Farhadi, M.; Jafari, M. A comprehensive review on double pipe heat exchangers. Appl. Therm. Eng. 2017, 110, 1075–1090.
[2]. Setareh, M.; Sa_ar-Avval, M.; Abdullah, A. Experimental and numerical study on heat transfer enhancement using ultrasonic vibration in a double-pipe heat exchanger. Appl. Therm. Eng. 2019, 159, 113867.
[3]. Khudheyer, Ahmed F., Al-Abbas, A.H., Carutasiu, M.-B., Necula, H. Turbulent heat transfer for internal flow of ethylene glycol-AL2O3 nanofluid in a spiral grooved tube with twisted tape inserts. Journal of Thermal Engineering, 2021, 7(4), pp. 761–772.
[4]. Abbas, A.S., Mahmoud, M.S., Khudheyer, Ahmed F., Improvement of heat transfer for airflow through a solar air heater channel with cutoff desecrate baffles. Journal of Green Engineering, 2020, 10(7), pp. 4292–4308
[5]. MohanadSalih Mahdi, Ahmed F. Khudheyer, 2021, "Central Receivers Design in Concentrated Solar Thermal Power Plants: A review"IOP Conference Series: Materials Science and Engineering, 1094(1).
[6]. Khudheyer, A.F., Hasan, Z.H., Effect of the Fins Configuration on Natural Convection Heat Transfer Experimentally and Numerically, International Journal of Energy and Environment, vol. 6, pp: 607-628, 2015.
[7]. Ahmed F. Khudheyer, Suha K. Jebir, and Mazin Y. Abdul-Kareem, 2022, "Thermal performance for solar trough collector with double absorber pipes," International Journal of Mechanical Engineering, 7(1), 571-578.
[8]. Ahmed F. Khudheyer, Mazin Y. Abdul-Kareem , Suha K. Jebir, 2022, "Assessment of a parabolic trough collector's thermophysical performance" International Journal of Mechanical Engineering, 7(1), pp. 620-630.
[9]. Mahmoud Sh. Mahmoud, Khudheyer, Ahmed F. 2020. "A Novel design of the solar central receiver to improve the performance of the central solar power tower plant". IOP Conf. Ser.: Mater. Sci. Eng. 928 022003. doi:10.1088/1757-899X/928/2/022003
[10]. Khudheyer, Ahmed. F., Numerical investigation and exergetic analysis of convergent-divergent absorber tube in concentrated solar trough. Journal of Green Engineering, 2020, 10(10), pp. 8083–8104.
[11]. Song, K.W.; Wang, L.; Hu, Y.J.; Liu, Q. Flow symmetry and heat transfer characteristics of winglet vortex generators arranged in common flow up configuration. Symmetry 2020, 12, 247.
[12]. Ali AbduladheemHilal and Ahmed F. Khudheyer., Fluid flow and heat transfer features in a twisting elliptical tube. *International Journal of Mechanical Engineering*, V(7), No.1, 5574 – 5583, 2022.
[13]. Ahmed F. Khudheyer, Suha K. Jebir, and Mazin Y. Abdul-Kareem, 2021, "The use of a parabolic trough concentrator at intermediate temperature to thermal commercial progressions," International Journal of Latest Engineering and Management Research (IJLEMR), 6(6), 22−26.
[14]. Suha K. Jebir, Ahmed F. Khudheyer, Noor Y. Abbas, 2021, "Effect of Different Nanofluids on Solar Radiation Absorption," Journal of Mechanical Engineering Research and Developments, 44(1),190-206.
[15]. Suha K. Jebir, 2021, "Enhancement of energy transferred in a pipe that equipped with a fixed Spiral Tape – Review," International Journal of Advances in Engineering and Management (IJAEM), 3(10), 314-317.
[16]. Jebir, Suha Kareem, Abbas, Noor Y., Khudheyer, Ahmed F., Effect of different nanofluids on solar radiation absorption. Journal of Mechanical Engineering Research and Development, 2020, 44(1), pp. 190–206
[17]. Mustafa W. K. Jaber.AnsamAdil Mohammed; Ahmed F. Khudheyer. Optimizing the size for Solar Parabolic Trough Concentrator numerically. International Journal of Mechanical Engineering. 2022, v.7, no. 1, 610–615.
[18]. Mahmoud, S.; Abbas, A.; and Khudheyer, AhmedF.,2020. "Solar parabolic trough collector tube heat transfer analysis with internal conical pin fins". Journal of Green Engineering, 10(10), 7422-7436.
[19]. Mahmoud Sh. Mahmoud, Ahmed F. Khudheyer and Qusay J. Abdul Ghafoor, 2020. "A Novel design of the solar central receiver to improve the performance of the central solar power tower plant". IOP Conf. Ser.: Mater. Sci. Eng. 928
[20]. Esmaeilzadeh, E.; Almohammadi, H.; Nokhosteen, A.; Motezaker, A.; Omrani, A.N. Study on heat transfer and friction factor characteristics of -Al2O3/water through circular tube with twisted tape inserts with different thicknesses. Int. J. Therm. Sci. 2014, 82, 72–83.

[21]. Man, C.Z.; Yao, J.Y.; Wang, C. The experimental study on the heat transfer and friction factor characteristics in tube with a new kind of twisted tape insert. Int. Commun. Heat Mass Transf. 2016, 75, 124–129.
[22]. Pourahmad, S.; Pesteei, S.M. E_ectiveness-NTU analyses in a double tube heat exchanger equipped with wavy strip considering various angles. Energy Convers. Manag. 2016, 123, 462–469.
[23]. Zhang, Z.; Ding, Y.M.; Guan, C.F.; Yan, H.; Yang, W.M. Heat transfer enhancement in double-pipe heat exchanger by means of rotor-assembled strands. Chem. Eng. Process. Process Intensif. 2012, 60, 26–33.
[24]. Bhadouriya, R.; Agrawal, A.; Prabhu, S.V. Experimental and numerical study of fluid flow and heat transfer in an annulus of inner twisted square duct and outer circular pipe. Int. J. Therm. Sci. 2015, 94, 96–109.
[25]. Bashtani, I.; Esfahani, J.A. "-NTU analysis of turbulent flow in a corrugated double pipe heat exchanger: A numerical investigation. Appl. Therm. Eng. 2019, 159, 113886.
[26]. Zambaux, J.A.; Harion, J.L.; Russeil, S.; Bouvier, P. The e_ect of successive alternating wall deformation on the performance of an annular heat exchanger. Appl. Therm. Eng. 2015, 90, 286–295.
[27]. Wang, W.; Zhang, Y.; Lee, K.S.; Li, B. Optimal design of a double pipe heat exchanger based on the outward helically corrugated tube. Int. J. Heat Mass Transf. 2019, 135, 706–716.
[28]. Gorman, J.M.; Krautbauer, K.R.; Sparrow, E.M. Thermal and fluid flow first-principles numerical design of an enhanced double pipe heat exchanger. Appl. Therm. Eng. 2016, 107, 194–206.
[29]. Qi, C.; Luo, T.; Liu, M.N.; Fan, F.; Yan, Y.Y. Experimental study on the flow and heat transfer characteristics of nanofluids in double-tube heat exchangers based on thermal efficiency assessment. Energy Convers. Manag.2019, 197, 111877.
[30]. Sadeghianjahromi, A.; Kheradmand, S.; Nemati, H. Developed correlations for heat transfer and flow friction characteristics of louvered finned tube heat exchangers. Int. J. Therm. Sci. 2018, 129, 135–144.
[31]. Luo, C.; Wu, S.; Song, K.W.; Hua, L.; Wang, L.B. Thermo-hydraulic performance optimization of wavy fin heat exchanger by combining delta winglet vortex generators. Appl. Therm. Eng. 2019, 163, 114343.
[32]. Luo, C.; Song, K.W.; Tagawa, T.; Wu, X.; Wang, L.B. Thermal performance of a zig-zag channel formed by two wavy fins mounted with vortex generators. Int. J. Therm. Sci. 2020, 153, 106361.
[33]. Song, K.W.; Shi, W.N.; Wu, X.; Wang, L.B. Characteristics of flow symmetry and heat transfer of winglet pair in common flow down configuration. Symmetry 2020, 12, 209.
[34]. Song, K.W.; Tagawa, T.; Chen, Z.H.; Zhang, Q. Heat transfer characteristics of concave and convex curved vortex generators in the channel of plate heat exchanger under laminar flow. Int. J. Therm. Sci. 2019, 137, 215–228.
[35]. Song, K.W.; Wang, L.B. Effects of longitudinal vortex interaction on periodically developed flow and heat transfer of fin-and-tube heat exchanger. Int. J. Therm. Sci. 2016, 109, 206–216.